crystals

MDPI

Article

Features of the Phase Formation of Cr/Mn/Fe/Co/Ni/Cu Codoped Bismuth Niobate Pyrochlore

Nadezhda A. Zhuk [1,*], Boris A. Makeev [2], Maria G. Krzhizhanovskaya [3], Sergey V. Nekipelov [4,*], Danil V. Sivkov [4] and Ksenia A. Badanina [1]

[1] Institute of Natural Sciences, Syktyvkar State University, Oktyabrsky Prospect, 55, Syktyvkar 167001, Russia; badanina-ksenia@mail.ru
[2] Institute of Geology of the Komi Science Center UB RAS, Pervomaiskaya St. 48, Syktyvkar 167982, Russia; makboris@mail.ru
[3] Institute of Earth Sciences, Saint Petersburg State University, University Emb. 7/9, St. Petersburg 199034, Russia; krzhizhanovskaya@mail.ru
[4] Institute of Physics and Mathematics of the Komi Science Center UB RAS, Oplesnina St. 4, Syktyvkar 167982, Russia; danjorno@yandex.ru
* Correspondence: nzhuck@mail.ru (N.A.Z.); nekipelovsv@mail.ru (S.V.N.)

Abstract: The phase formation process of $Bi_2Cr_{1/6}Mn_{1/6}Fe_{1/6}Co_{1/6}Ni_{1/6}Cu_{1/6}Nb_2O_{9+\Delta}$ containing 3d-ions of transition elements in equimolar quantities was studied in a wide temperature range (400–1050 °C). The complex oxide crystallizes in the structural type of pyrochlore (sp. gr. Fd-3m:2, a = 10.4937(2) Å). The investigation of the multi-element pyrochlore phase formation process showed that the synthesis goes through a series of successive stages, during which the transition from Bi-rich to Bi-depleted compounds takes place. The predecessor of the pyrochlore phase is bismuth orthorhombic modification orthoniobate (α-$BiNbO_4$) with an equimolar ratio of Bi(III)/Nb(V) ions. The pyrochlore phase is formed as a result of bismuth orthoniobate doping with transition element ions. The complex oxides $Bi_{14}CrO_{24}$, $Bi_{25}FeO_{40}$, $BiNbO_4$, and $Bi_5Nb_3O_{15}$ appeared as intermediate phases during the synthesis. The interaction between the initial oxide precursors is fixed at temperatures above 500 °C. The phase transition of α-Bi_2O_3 into β-Bi_2O_3 near 500 °C is observed. Varying the heat treatment duration at each synthesis step did not qualitatively change the phase composition of the sample but had an effect on the quantitative phase ratio. Phase-pure pyrochlore of the given composition by solid-phase synthesis method can be obtained at a temperature no lower than 1050 °C. Ceramics are characterized by low-porous dense microstructure with blurred outlines of grain boundaries.

Keywords: pyrochlore; bismuth tantalate; doping; transitional 3d elements; phase formation

check for updates

Citation: Zhuk, N.A.; Makeev, B.A.; Krzhizhanovskaya, M.G.; Nekipelov, S.V.; Sivkov, D.V.; Badanina, K.A. Features of the Phase Formation of Cr/Mn/Fe/Co/Ni/Cu Codoped Bismuth Niobate Pyrochlore. *Crystals* **2023**, *13*, 1202. https://doi.org/10.3390/cryst13081202

Academic Editor: Zhonghua Yao

Received: 30 June 2023
Revised: 28 July 2023
Accepted: 30 July 2023
Published: 2 August 2023

Copyright: © 2023 by the authors. Licensee MDPI, Basel, Switzerland. This article is an open access article distributed under the terms and conditions of the Creative Commons Attribution (CC BY) license (https://creativecommons.org/licenses/by/4.0/).

1. Introduction

Sustained interest in synthetic pyrochlores is due to the wide range of their practically useful properties. The most promising are dielectric properties (low dielectric losses and high dielectric permittivity, tunable temperature coefficient of capacitance) and photocatalytic properties [1–3]. A useful addition is the relatively low synthesis temperature and thermal stability of pyrochlores [4]. The crystal structure of pyrochlores is traditionally described by the chemical formula $A_2B_2O_6O'$, in which two interpenetrating cationic sublattices A_2O' and B_2O_6 are distinguished [5,6]. The cationic sublattice A_2O' is similar to the structure of antichristobalite; the B_2O_6 sublattice forms a three-dimensional framework of octahedrons connected by their vertices. The B octahedral positions are occupied by relatively small cations (Ta^{5+}, Ru^{4+}, Zr^{4+}, Nb^{5+}), and the larger ions (Bi^{3+}, Ln^{3+}, Ca^{2+}) are distributed in the eight coordinated positions A. In bismuth pyrochlores, the Bi^{3+} cations shift from ideal 16d positions, which are typical for A cations in ideal pyrochlore structure, to 96h or 96g positions due to stereoactive $6s^2$ lone pair of electrons. This leads to the formation of pyrochlores with an unfilled bismuth sublattice. Meanwhile, the distortion

of the octahedral sublattice arising during doping by the 3d-element atoms leads to the partial distribution of the transition element ions in the bismuth(III) position [5–10]. The flexibility of pyrochlore crystal structure to substitutions of cations in bismuth/niobium sublattices and to oxygen vacancies in A_2O' sublattice allows their functional properties to be adjusted.

Mixed pyrochlores based on bismuth antimonate, tantalate, and niobate [7–15] are actively studied due to their promising electrical and catalytic properties. A feature of the pyrochlores under consideration is a vacant bismuth sublattice and the placement of heterovalent ions of transition elements (Cu, Co, Mn, Zn), which are disproportionate to the B sublattice ions into the bismuth sublattice. This causes relaxation processes in ceramics [15–19]. Studies of bismuth tantalate-based pyrochlores containing transition 3d ions (Cu, Ni, Fe, Cr, Co, Zn) [10–12,14,17,20–23] have shown the formation of porous ceramics with low dielectric losses and moderate dielectric permittivity values. Copper-containing bismuth tantalates exhibiting multiple dielectric relaxation at temperatures above room temperature are characterized by a specific behavior [20,21]. $Bi_{2.48+y}Cu_{1.92-x}Ta_{3.6+x-y}O_{14.6+3x/2-y;}$ solid solutions [12] exhibit moderate dielectric constants of 60–80 and dielectric losses (tan δ = 0.01–0.20, RT, 1 MHz). As shown in [24], iron-containing pyrochlores in the Bi_2O_3-Fe_2O_3-Nb_2O_5 system exhibit high values of dielectric constant 141–151 and dielectric loss 0.2 at 30 °C and 1 MHz [24]. Iron-containing pyrochlores $Bi_{3.36}Fe_{2.08+x}Ta_{2.56-x}O_{14.56-x}$ ($-0.32 \leq x \leq 0.48$) based on bismuth tantalate show lower values of dielectric constant ~78–92 and dielectric loss tangent $\sim 10^{-1}$ (MHz, ~30 °C) [14], which is due to the high porosity of ceramics. Magnesium-containing pyrochlores $Bi_{3+5/2x}Mg_{2-x}Ta_{3-3/2x}O_{14-x}$ ($0.12 \leq x \leq 0.22$) are characterized by close values of ε ~70–85 and a low dielectric loss tangent δ $\sim 10^{-3}$ at 1 MHz and 30 °C [25]. For pyrochlore $Bi_{1.5}ZnTa_{1.5}O_7$, the dielectric permittivity is 58, dielectric loss is 0.0023 at 30 °C and 1 MHz; temperature coefficient of capacitance (TCC) 156 ppm/°C in the range of 30–300 °C at a frequency of 1 MHz [26,27]. The electrical characteristics of cobalt pyrochlores are comparable to those of nickel- and magnesium-containing preparations [10]. For magnesium pyrochlore $Bi_2MgTa_2O_9$, the permittivity and dielectric loss tangent are 20 and $2 \cdot 10^{-3}$ (RT, 1 MHz) [4], and for nickel pyrochlore permittivity and dielectric loss, tangents are 32 and $6 \cdot 10^{-2}$ at room temperature and frequency 1 MHz, respectively [11]. As shown in [28], $Bi_{1.4}(Mg_{1-x}Ni_x)_{0.7}Ta_{1.4}O_{6.3}$ (x = 0.3, 0.5, 0.7) samples are insulators and have high activation energies of ~2.0 eV; moderately high dielectric constants ~24–28 and dielectric losses ~0.002 at 1 MHz and 21 °C.

The study of the phase formation process of multielement bismuth tantalate with pyrochlore structure revealed a number of peculiarities [29]. The most significant is the recognition of α-$BiTaO_4$ as an important intermediate in the synthesis of the pyrochlore phase [29–31]. An uneven change in the parameter of the pyrochlore cell constant associated with the formation of nonstoichiometric pyrochlore was noted [31]. The formation of intermediate synthesis products containing Cr(VI) ions was established [30]. The influence of zinc and magnesium ions on the phase relations during the synthesis of pyrochlore was shown [30,31].

In the present work, we aimed to identify similarities and differences in the phase formation stages of multielement tantalates and niobates with pyrochlore structure. This allowed us to note the specific features of the phase formation associated with the nature of niobium(V) and tantalum(V) oxides to determine the optimal conditions for the ceramic synthesis. In this regard, the presented work determines the synthesis conditions and the phase formation stages of multielement pyrochlore based on bismuth niobate and analyzes the phase composition of the samples at each synthesis stage.

2. Experimental Part

Multielement pyrochlore was synthesized by standard ceramic technology from the corresponding oxides of Bi(III), Nb(V), Ni(II), Co(II,III), Cu(II), Mn(III), Cr(III), Fe(III) of analytical grade. The stoichiometric mixture of precursors was finely ground and homogenized in a jasper mortar for one hour. The resulting homogeneous charge was

compacted in the form of disks using a plexiglas mold. Air calcination of samples was carried out step by step in the temperature range of 400–1050 °C (step 50 °C) for 10 and 15 h at each stage of thermal treatment. After each stage of calcination, the samples were reground again and pressed in the form of disks. X-ray powder diffraction phase analysis was performed using a Shimadzu 6000 X-ray diffractometer (CuKα radiation; 2θ = 10–60°; scanning speed 2.0°/min). The unit cell parameters have been refined by the Topas 5.0 program employing the Pawley approach and using CSD software [32]. The background was described by 12 Chebyshev polynomials, and the peak shape was modeled by the Thompson–Cox–Hastings pseudo-Voigt function. Surface morphology studies and local quantitative elemental analysis of the samples were performed using a scanning electron microscope (Tescan VEGA 3LMN) and an energy-dispersive X-ray spectrometer (INCA Energy 450).

3. Results and Discussion

According to the X-ray powder diffraction phase analysis data, the sample with the $Bi_2Cr_{1/6}Mn_{1/6}Fe_{1/6}Co_{1/6}Ni_{1/6}Cu_{1/6}Nb_2O_{9+\Delta}$ composition is single-phase and crystallized in the structural type of pyrochlore (sp. gr. Fd-3m, R_{br} = 0.234) (Figure 1) [5,6]. Its unit cell parameter a = 10.4937(2) Å is comparable with the bismuth-deficient tantalum pyrochlore analogue $Bi_{2-1/3}Cr_{1/6}Mn_{1/6}Fe_{1/6}Co_{1/6}Ni_{1/6}Cu_{1/6}Ta_2O_{9+\Delta}$ (a = 10.48106 Å) [33]. The images of the sample surface obtained by means of scanning electron microscopy in the mode of elastically reflected electrons (BSE mode) do not contain areas of contrast in color associated with the presence of impurity phases. Energy dispersive spectroscopy (EDS) analysis showed (Figure S1) (see Supplementary Materials) that the chemical composition of the sample is close to the specified one.

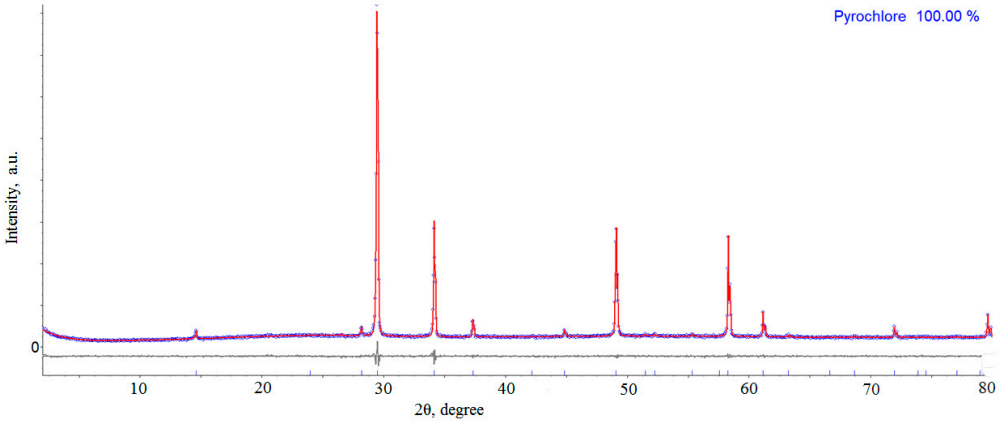


Figure 1. X-ray powder diffraction patterns of the $Bi_2Cr_{1/6}Mn_{1/6}Fe_{1/6}Co_{1/6}Ni_{1/6}Cu_{1/6}Nb_2O_{9+\Delta}$ synthesized at 1050 °C.

Since the tantalum analog of the $Bi_2Cr_{1/6}Mn_{1/6}Fe_{1/6}Co_{1/6}Ni_{1/6}Cu_{1/6}Nb_2O_{9+\Delta}$ composition is multiphase and contains an admixture of the bismuth orthotantalate $BiTaO_4$, one can conclude that the tantalum and niobium pyrochlore have a different set of heterovalent transition element ions. This refers to the ions of each transition element in the pyrochlore composition. For example, for manganese, there may be a set of Mn(II), Mn(III), and Mn(IV) ions. The difference can appear in the quantitative ratios of one element's ions. Since the $BiTaO_4$ impurity accompanies the bismuth tantalate-based composition, this may mean that there are more transition element ions disproportionate to Ta(V) ions in the tantalum pyrochlore than in the niobium one, while the ionic radii of niobium and tantalum are equal ($R(Ta^{5+})_{cn\text{-}6} = R(Nb^{5+})_{cn\text{-}6}$ = 0.064 nm) [34].

The process of $Bi_2Cr_{1/6}Mn_{1/6}Fe_{1/6}Co_{1/6}Ni_{1/6}Cu_{1/6}Nb_2O_{9+\Delta}$ phase formation was studied by comparing the phase composition of samples calcined every 50 °C in the temperature range of 400–1050 °C. Analysis of phase composition and microstructure and

elemental mapping of samples were performed at each stage of heat treatment. X-ray powder diffraction patterns of calcined samples in the temperature intervals of 400–650 °C and 650–1050 °C are shown in Figures 2 and 3.

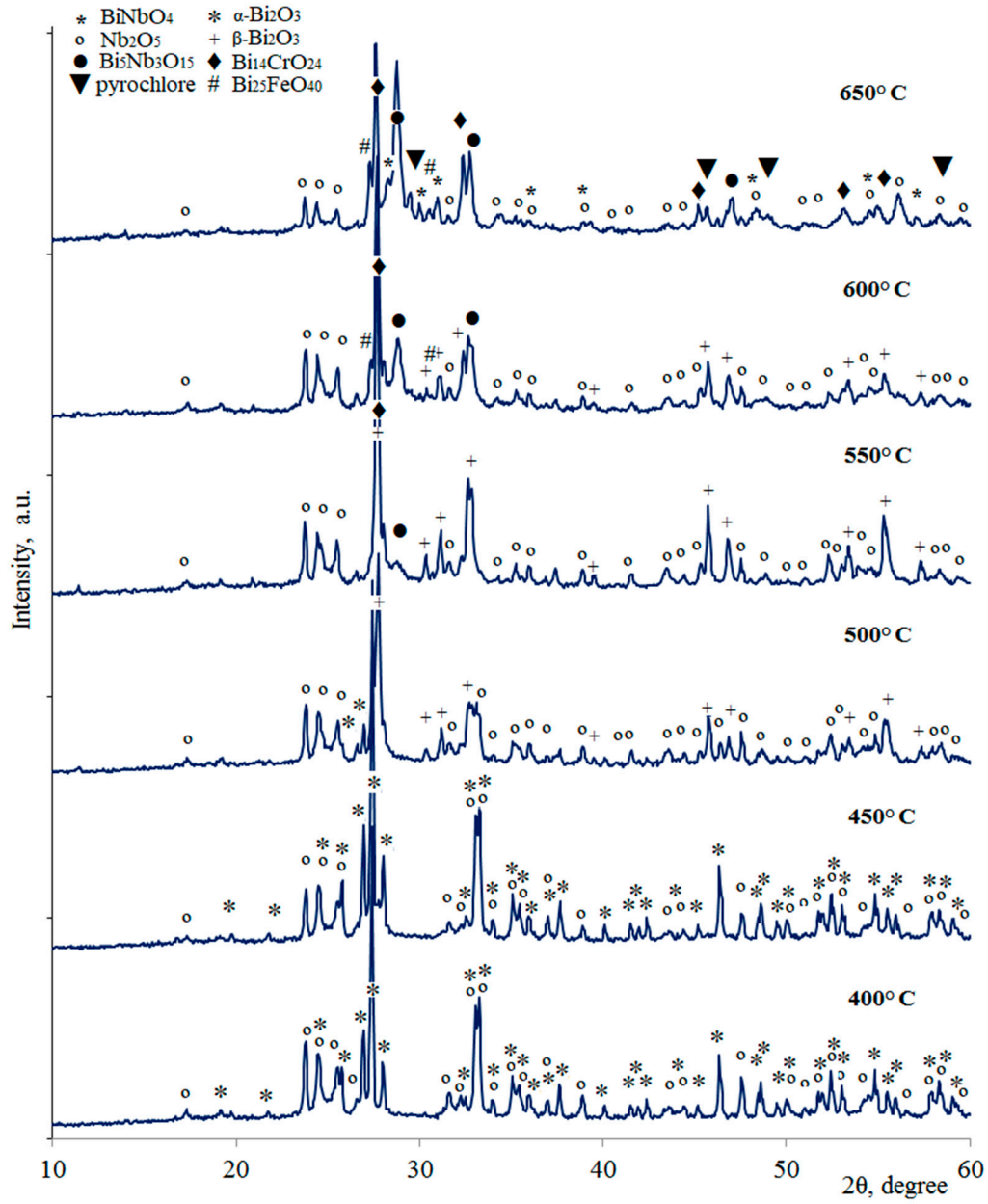


Figure 2. X-ray powder diffraction patterns of the $Bi_2Cr_{1/6}Mn_{1/6}Fe_{1/6}Co_{1/6}Ni_{1/6}Cu_{1/6}Nb_2O_{9+\Delta}$ calcined at a step change in temperature from 400 to 650 °C (10 h).

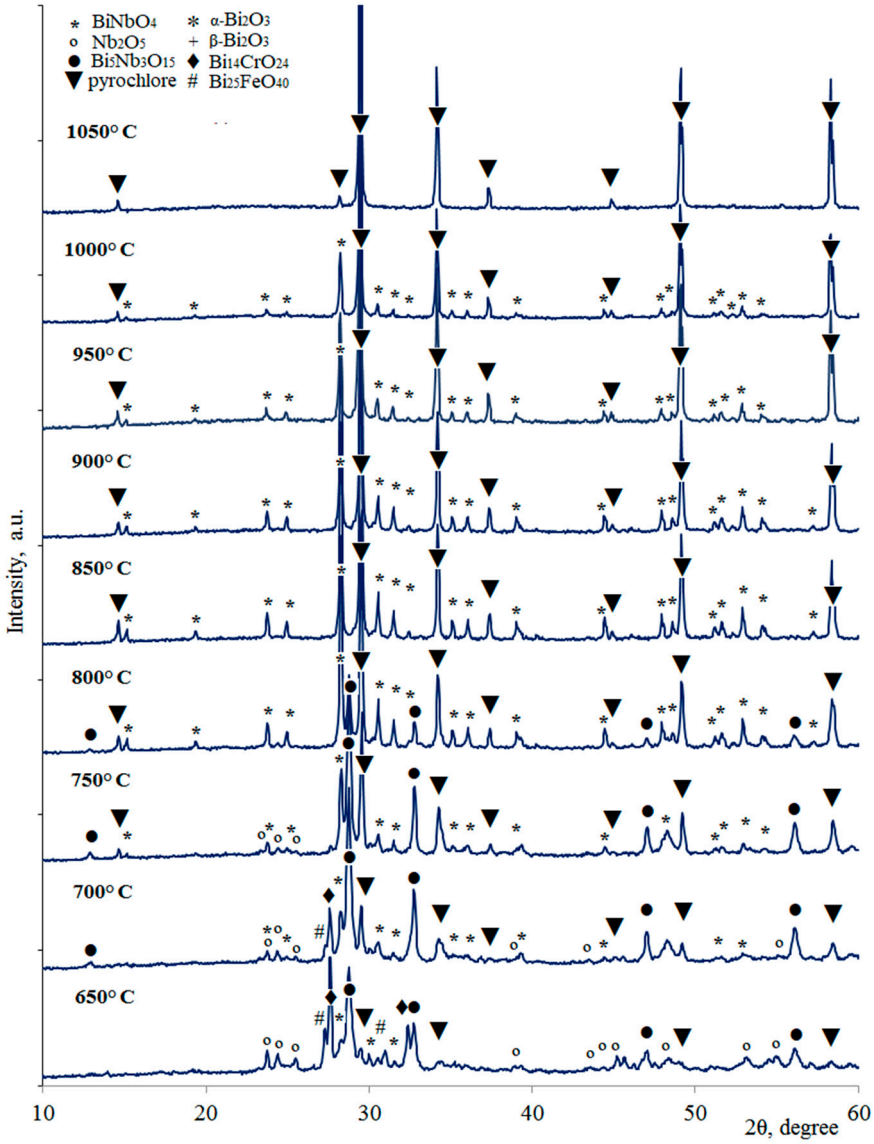


Figure 3. X-ray powder diffraction patterns of the $Bi_2Cr_{1/6}Mn_{1/6}Fe_{1/6}Co_{1/6}Ni_{1/6}Cu_{1/6}Nb_2O_{9+\Delta}$ calcined at a step change in temperature from 650 to 1050 °C (for 10 h).

The phase composition of the sample significantly depends on the calcination temperature. Table 1 contains the results of studies of the phase composition in the sample by X-ray powder diffraction patterns. The results of elemental mapping (for all elements—Bi, Nb, O, atoms of 3d elements) of samples calcined in the temperature interval of 650–1050 °C (in 50 °C increments) are shown in Figure 4 and Figure S2.

Table 1. $Bi_2Cr_{1/6}Mn_{1/6}Fe_{1/6}Co_{1/6}Ni_{1/6}Cu_{1/6}Nb_2O_{9+\Delta}$ phase composition depending on the synthesis temperature.

Synthesis Temperature, °C	Phase Composition
400	η-Nb_2O_5, α-Bi_2O_3
450	η-Nb_2O_5, α-Bi_2O_3
500	η-Nb_2O_5, α-Bi_2O_3, β-Bi_2O_3
550	η-Nb_2O_5, β-Bi_2O_3, $Bi_5Nb_3O_{15}$, $Bi_{14}CrO_{24}$
600	η-Nb_2O_5, β-Bi_2O_3,$Bi_5Nb_3O_{15}$, $Bi_{14}CrO_{24}$, $Bi_{25}FeO_{40}$
650	$Bi_{25}FeO_{40}$,β-Nb_2O_5, $Bi_5Nb_3O_{15}$, $Bi_{14}CrO_{24}$, $BiNbO_4$, pyrochlore

Table 1. *Cont.*

Synthesis Temperature, °C	Phase Composition
700	$Bi_{25}FeO_{40}$(traces),β-Nb_2O_5, $Bi_5Nb_3O_{15}$, $Bi_{14}CrO_{24}$, $BiNbO_4$, pyrochlore
750	β-Nb_2O_5(traces), $Bi_{14}CrO_{24}$(traces), $Bi_5Nb_3O_{15}$, $BiNbO_4$, pyrochlore
800	$Bi_5Nb_3O_{15}$(traces), $BiNbO_4$, pyrochlore
850	pyrochlore (68), $BiNbO_4$ (32)
900	pyrochlore (70), $BiNbO_4$ (30)
950	pyrochlore (76), $BiNbO_4$ (24)
1000	pyrochlore (89), $BiNbO_4$ (11)
1050	$Bi_2Cr_{1/6}Mn_{1/6}Fe_{1/6}Co_{1/6}Ni_{1/6}Cu_{1/6}Nb_2O_{9+\Delta}$ (100)

Note. The numbers in parentheses indicate the mass fraction (wt.%) of the phases in the sample.

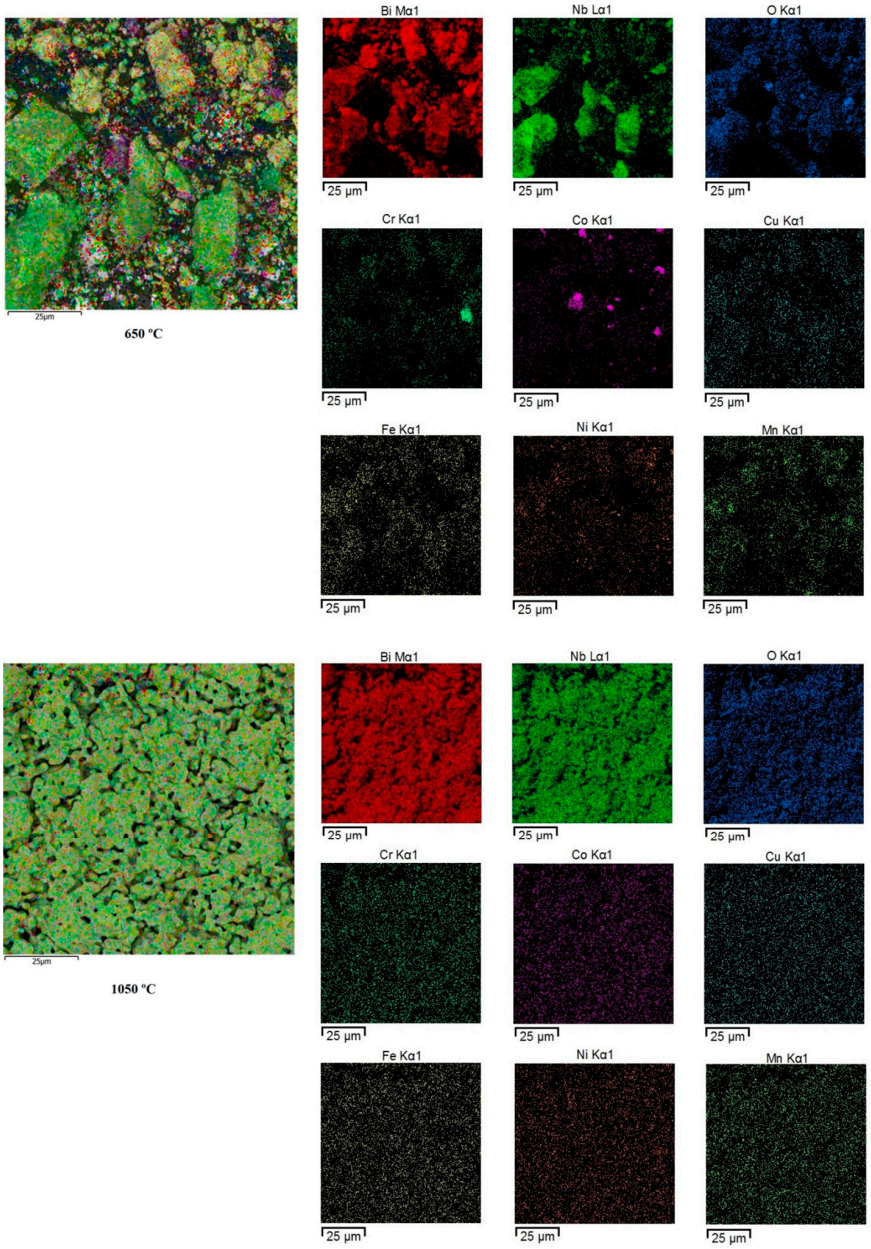


Figure 4. EDX elemental mapping of the $Bi_2Cr_{1/6}Mn_{1/6}Fe_{1/6}Co_{1/6}Ni_{1/6}Cu_{1/6}Nb_2O_{9+\Delta}$ samples, synthesized at temperatures 650 and 1050 °C.

The data of X-ray powder diffraction phase analysis show that in the temperature range of 400–450 °C the phases of the initial precursors coexist, in particular, the Bragg reflections of monoclinic η-Nb_2O_5 (sp. gr P2/m, PDF Card-01-071-0005) [35] and α-Bi_2O_3 [36,37] phases are clearly observed. The phase transition from monoclinic α-Bi_2O_3 (sp. gr. P21/c, PDF Card-01-070-8243) to tetragonal β-Bi_2O_3 phase (sp. gr. P-421c, PDF Card-01-077-5341) occurs near 500 °C.

At 550 °C, in addition to the Bragg reflections of β-Bi_2O_3 and η-Nb_2O_5 oxides, the Bragg reflections of the interaction products of the initial precursors—$Bi_5Nb_3O_{15}$ (sp. gr. P4/mmm, PDF Card-00-055-0528) [38] and chromium(VI) compound $Bi_{14}CrO_{24}$ (sp. gr. I4/m, PDF Card-01-070-4457) [39] are detected. The formation of intermediate chromium(VI) compounds was observed when pyrochlores of $Bi_2Mg(Zn)_{1-x}Cr_xTa_2O_{9.5-\Delta}$ up to 700 °C were obtained [30].

X-ray powder diffraction patterns of samples calcined at 600 °C contain sillenite reflexes $Bi_{25}FeO_{40}$ (sp. gr. I23, PDF Card-00-046-0416) [40]. At 650 °C the bismuth oxide phase does not manifest itself, and the niobium oxide content decreases; at the same time, the $Bi_5Nb_3O_{15}$, $Bi_{14}CrO_{24}$, and $Bi_{25}FeO_{40}$ content increases, as well as the $BiNbO_4$ and pyrochlore phases first appear. An increase or decrease in the phase content in the sample was judged from the change in the relative intensities of the Bragg reflections. In Table 1, in the temperature range from 650 to 1000 °C, the presence of the pyrochlore phase is noted. The composition of the phase is unknown because the synthesis is incomplete. We believe that nonstoichiometric pyrochlore is formed at this stage of the synthesis. At 700 °C, the intensity decreases, and at 800 °C and 750 °C, the reflexes of $Bi_{14}CrO_{24}$ and $Bi_{25}FeO_{40}$ phases disappear, which may be related to the intensive synthesis of pyrochlore. No niobium oxide reflexes are detected in X-ray powder diffraction patterns of samples synthesized at 800 °C, and $Bi_5Nb_3O_{15}$ is not present at 850 °C. On this basis, one can note the chemical inertness of niobium oxide compared to bismuth one, which does not form an independent phase already at 650 °C. During high-temperature treatment of the sample, the transition from Bi-rich to Bi-depleted compounds is observed. The intermediate phase in the pyrochlore synthesis is $Bi_5Nb_3O_{15}$, whereas the Bi-rich analog in the bismuth tantalate-based pyrochlore synthesis is Bi_3TaO_7 (sp. gr Fm-3m, PDF Card-01-076-8514) [41], while its isostructural analogue is Bi_3NbO_7 [42,43]. This is partly due to the fact that the $Bi_5Ta_3O_{15}$ compound is not stable. Moreover, one can assume that the reactivity of oxides of transition elements, such as chromium(III) or iron(III), is higher than that of niobium(V), so bismuth oxide is consumed primarily and in significant amounts by interacting with them. From 850 °C to 1050 °C the samples are biphasic and consist of pyrochlore and bismuth orthoniobate of α-$BiNbO_4$ (Pnna, PDF Card-01-072-7513) modification [44,45]. It should be noted that the $BiNbO_4$ fraction begins to decrease in the samples calcined at 950 °C and higher, which is associated with the activation of the reactivity of transition element oxides and pyrochlore synthesis. The quantitative ratios of pyrochlore and bismuth orthoniobate phases in the range of 850–1000 °C are shown in Table 1. The precursors—oxides of transition elements—are not detected on the samples' X-ray powder diffraction patterns due to their low content in the initial charge and high reactivity. In order to investigate the distribution of transition element ions, the elemental mapping of samples synthesized at 650–1050 °C was carried out (Figure 4 and Figure S2). According to the elemental mapping data, transition element ions are unevenly distributed in the sample synthesized at 650 °C due to its multiphase. A more even distribution of elements is fixed in the samples calcined above 700–750 °C due to the active formation of the pyrochlore phase as a result of the interaction of bismuth niobate and oxides of transition elements. At 1050 °C, ions are uniformly distributed over the sample surface. Meanwhile, the distribution of cobalt and chromium ions should be noted. When at 650 °C, their distribution over the surface is independent, then, starting from the calcination at 750 °C, they form single centers of concentration. This may indicate the formation of a complex chromium-cobalt-bearing oxide (Figure 5).

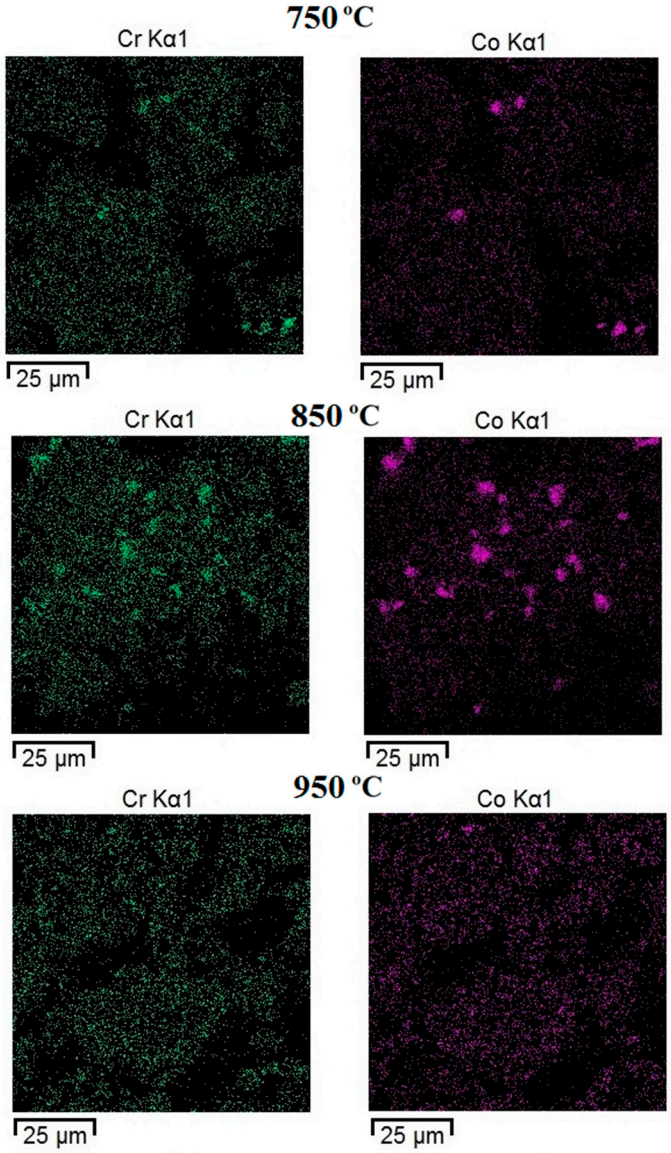


Figure 5. EDX elemental mapping (Co and Cr) of the $Bi_2Cr_{1/6}Mn_{1/6}Fe_{1/6}Co_{1/6}Ni_{1/6}Cu_{1/6}Nb_2O_{9+\Delta}$, samples, synthesized at temperatures from 750, 850 and 950 °C.

This indicates that of the oxides of the other six transition elements, only the oxides of cobalt and chromium interact to form a complex oxide. EDS analysis showed that the stoichiometry of such a compound is close to the spinel formula $CrCo_2O_4 = Co^{2+}Cr^{3+}Co^{3+}O_4$ [45]. The occurrence of the complex cobalt oxide impurity is explained by its small reactivity, which was noted in [29]. A single-phase sample with uniform distribution of all ions over the sample surface was obtained at 1050 °C, which is confirmed by X-ray powder diffraction phase analysis and elemental mapping data. It should be noted that an increase in sample calcination at each synthesis stage from 10 to 15 h did not lead to qualitative differences in the phase composition of the samples; only the quantitative phase ratios changed. This conclusion was made on the basis of the phase analysis of samples calcined for 15 h at each stage of heat treatment in the range of 650–1050 °C (with a step of 50 °C). All X-ray powder diffraction patterns of the samples are shown in Figure S3. The evaluation of the relative intensities of Bragg reflections of pyrochlore and orthoniobate phases showed that the content of impurity-$BiNbO_4$ was greater in the samples calcined for 15 h (Figure S3).

Apparently, the prolonged calcination of the samples (15 h) contributed to ceramic grain enlargement and hindered the interaction of precursors.

Microphotographs of the synthesized samples' surfaces in the temperature range of 650–1050 °C are shown in Figure 6. The heterogeneous microstructure with different grains and inclusions of impurity phases is characteristic of samples calcined at 650–1000 °C. The low-porous, dense microstructure is formed in the sample synthesized at a temperature of 1050 °C. Grain intergrowth with the formation of large crystallites and the formation of a monolithic microstructure are observed in ceramics in contrast to pyrochlores based on bismuth tantalate [30,31].

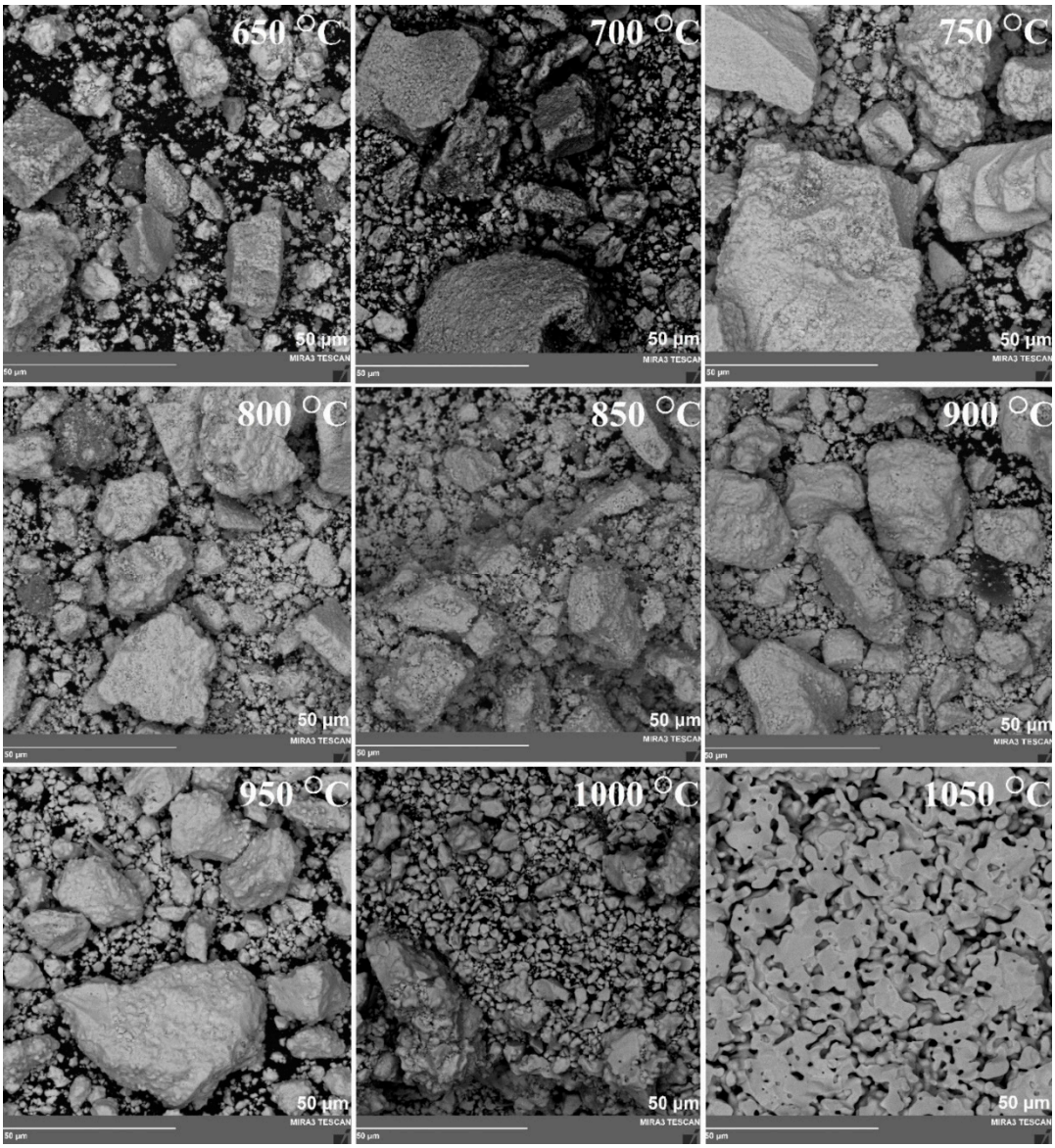


Figure 6. Surface micrographs of the $Bi_2Cr_{1/6}Mn_{1/6}Fe_{1/6}Co_{1/6}Ni_{1/6}Cu_{1/6}Nb_2O_{9+\Delta}$ samples, synthesized at temperatures from 650 and 1050 °C.

4. Conclusions

The multielement pyrochlore $Bi_2Cr_{1/6}Mn_{1/6}Fe_{1/6}Co_{1/6}Ni_{1/6}Cu_{1/6}Nb_2O_{9+\Delta}$ was synthesized by solid-phase reaction method. The phase-pure pyrochlore was obtained at 1050 °C. The microstructure of the sample is low-porous with implicit grain boundary outlines. The process of pyrochlore phase evolution in the temperature interval of 400–1050 °C is analyzed. A number of peculiarities of the phase formation process are revealed. The phase formation is a multistage process that ends at a temperature of 1050 °C with the synthesis of single-phase pyrochlore. The synthesis reaction of the pyrochlore phase con-

sists of the interaction of orthorhombic bismuth orthoniobate with oxides of transition elements. The interaction between oxides is fixed at temperatures above 500 °C. Near 500 °C bismuth oxide undergoes a phase transition of α-Bi_2O_3 to β-Bi_2O_3. The synthesis is a multistep process, and the transition of Bi-rich to Bi-depleted oxide compounds is observed. During the synthesis, intermediate compounds of $Bi_{14}CrO_{24}$ and $Bi_{25}FeO_{40}$ are formed. The duration of calcination (15 and 10 h at each synthesis stage) did not affect the phase composition but had an effect on the quantitative ratios of the phases in the sample.

Supplementary Materials: The following supporting information can be downloaded at: https://www.mdpi.com/article/10.3390/cryst13081202/s1, Figure S1: Microphotograph and EDS analysis of the $Bi_2Cr_{1/6}Mn_{1/6}Fe_{1/6}Co_{1/6}Ni_{1/6}Cu_{1/6}Nb_2O_{9+\Delta}$ sample, calcined at 1050 °C; Figure S2: EDS elemental mapping of the $Bi_2Cr_{1/6}Mn_{1/6}Fe_{1/6}Co_{1/6}Ni_{1/6}Cu_{1/6}Nb_2O_{9+\Delta}$ samples, synthesized at temperatures from 650 to 1050 °C; Figure S3: X-ray powder diffraction patterns of the $Bi_2Cr_{1/6}Mn_{1/6}Fe_{1/6}$-$Co_{1/6}Ni_{1/6}Cu_{1/6}Nb_2O_{9+\Delta}$ sample, calcined from 650 to 1050 °C (15 h).

Author Contributions: Conceptualization, N.A.Z.; Funding acquisition, S.V.N., D.V.S. and N.A.Z. Investigation, N.A.Z. and K.A.B.; Resources, M.G.K. and B.A.M.; Validation, N.A.Z.; Visualization, M.G.K., N.A.Z. and B.A.M.; Writing—original draft, N.A.Z. All authors have read and agreed to the published version of the manuscript.

Funding: The reported study was funded by Russian Science Foundation (project № 17-79-30071).

Data Availability Statement: Not applicable.

Acknowledgments: The authors thank the X-ray Diffraction Center SPSU for providing instrumental and computational resources.

Conflicts of Interest: The authors declare no conflict of interest.

References

1. Murugesan, S.; Huda, M.N.; Yan, Y.; Al-Jassim, M.M.; Subramanian, V. Band-Engineered Bismuth Titanate Pyrochlores for Visible Light Photocatalysis. *J. Phys. Chem.* **2010**, *114*, 10598–10605. [CrossRef]
2. Pandey, J.; Shrivastava, V.; Nagarajan, R. Metastable $Bi_2Zr_2O_7$ with Pyrochlore-like Structure: Stabilization, Oxygen Ion Conductivity, and Catalytic Properties. *Inorg. Chem.* **2018**, *57*, 13667–13678. [CrossRef] [PubMed]
3. Parrondo, J.; George, M.; Capuano, C.; Ayers, K.E.; Ramani, V. Pyrochlore electrocatalysts for efficient alkaline water electrolysis. *J. Mater. Chem. A* **2015**, *3*, 10819–10828. [CrossRef]
4. Zhuk, N.A.; Krzhizhanovskaya, M.G. Thermal expansion of bismuth magnesium tantalate and niobate pyrochlores. *Ceram. Int.* **2021**, *47*, 30099–30105. [CrossRef]
5. Subramanian, M.A.; Aravamudan, G.; Subba Rao, G.V. Oxide pyrochlores—A review. *Prog. Sol. St. Chem.* **1983**, *15*, 55–143. [CrossRef]
6. McCauley, R.A. Structural Characteristics of Pyrochlore Formation. *J. Appl. Phys.* **1980**, *51*, 290–294. [CrossRef]
7. Vanderah, T.A.; Lufaso, M.W.; Adler, A.U.; Levin, I.; Nino, J.C.; Provenzano, V.; Schenck, P.K. Subsolidus phase equilibria and properties in the system Bi_2O_3:$Mn_2O_{3\pm x}$:Nb_2O_5. *J. Solid State Chem.* **2006**, *179*, 3467–3477. [CrossRef]
8. Vanderah, T.A.; Siegrist, T.; Lufaso, M.W.; Yeager, M.C.; Roth, R.S.; Nino, J.C.; Yates, S. Phase Formation and Properties in the System Bi_2O_3:$2CoO_{1+x}$:Nb_2O_5. *Eur. J. Inorg. Chem.* **2006**, *2006*, 4908–4914. [CrossRef]
9. Lufaso, M.W.; Vanderah, T.A.; Pazos, I.M.; Levin, I.; Roth, R.S.; Nino, J.C.; Provenzano, V.; Schenck, P.K. Phase formation, crystal chemistry, and properties in the system Bi_2O_3–Fe_2O_3–Nb_2O_5. *J. Solid State Chem.* **2006**, *179*, 3900–3910. [CrossRef]
10. Zhuk, N.A.; Krzhizhanovskaya, M.G.; Koroleva, A.V.; Nekipelov, S.V.; Sivkov, D.V.; Sivkov, V.N.; Lebedev, A.M.; Chumakov, R.G.; Makeev, B.A.; Kharton, V.V.; et al. Spectroscopic characterization of cobalt doped bismuth tantalate pyrochlore. *Sol. St. Sci.* **2022**, *125*, 106820. [CrossRef]
11. Zhuk, N.A.; Krzhizhanovskaya, M.G.; Koroleva, A.V.; Nekipelov, S.V.; Kharton, V.V.; Sekushin, N.A. Thermal Expansion, XPS Spectra, and Structural and Electrical Properties of a New $Bi_2NiTa_2O_9$ Pyrochlore. *Inorg. Chem.* **2021**, *60*, 4924–4934. [CrossRef] [PubMed]
12. Chon, M.P.; Tan, K.B.; Khaw, C.C.; Zainal, Z.; Taufiq-Yap, Y.H.; Chen, S.K.; Tan, P.Y. Subsolidus phase equilibria and electrical properties of pyrochlores in the Bi_2O_3–CuO–Ta_2O_5 ternary system. *J. Alloys Compd.* **2016**, *675*, 116–127. [CrossRef]
13. Valant, M.; Suvorov, D. The Bi_2O_3-Nb_2O_5-NiO Phase Diagram. *J. Am. Ceram. Soc.* **2005**, *88*, 2540–2543. [CrossRef]
14. Jusoh, F.A.; Tan, K.B.; Zainal, Z.; Chen, S.K.; Khaw, C.C.; Lee, O.J. Novel pyrochlores in the Bi_2O_3-Fe_2O_3-Ta_2O_5 (BFT) ternary system: Synthesis, structural and electrical properties. *J. Mater. Res. Technol.* **2020**, *9*, 11022–11034. [CrossRef]

15. Egorysheva, A.V.; Ellert, O.G.; Gajtko, O.M.; Efimov, N.N.; Svetogorov, R.D.; Zubavichus, Y.V.; Grigorieva, A.V. The Bi_2O_3–Fe_2O_3–Sb_2O_5 system phase diagram refinement, $Bi_3FeSb_2O_{11}$ structure peculiarities and magnetic properties. *J. Solid State Chem.* **2015**, *225*, 278–284. [CrossRef]
16. Nino, J.C.; Lanagan, M.T.; Randall, C.A. Dielectric Relaxation in Bi_2O_3–ZnO–Nb_2O_5 Cubic Pyrochlore. *J. Appl. Phys.* **2001**, *89*, 4512–4516. [CrossRef]
17. Ang, C.; Yu, Z.; Yuon, H.J.; Randall, C.A. Low-Temperature Dielectric Relaxation in the Pyrochlore $(Bi_{3/4}Zn_{1/4})(Zn_{1/4}Ta_{3/4})O_7$ Compound. *Appl. Phys. Lett.* **2002**, *80*, 4807–4809. [CrossRef]
18. Kamba, S.; Porokhovskyy, V.; Pashkin, A. Anomalous Broad Dielectric Relaxation in $Bi_{1.5}Zn_{1.0}Nb_{1.5}O_7$ Pyrochlore. *Phys. Rev. B Condens. Matter.* **2002**, *66*, 1–8. [CrossRef]
19. Valant, M. Dielectric Relaxations in Bi_2O_3-Nb_2O_5-NiO Cubic Pyrochlores. *J. Am. Ceram. Soc.* **2009**, *92*, 955–958. [CrossRef]
20. Zhuk, N.A.; Krzhizhanovskaya, M.G.; Koroleva, A.V.; Sekushin, N.A.; Nekipelov, S.V.; Kharton, V.V.; Makeev, B.A.; Lutoev, V.P.; Sennikova, Y.D. Cu, Mg codoped bismuth tantalate pyrochlores: Crystal structure, XPS spectra, thermal expansion, and electrical properties. *Inorg. Chem.* **2022**, *61*, 4270–4282. [CrossRef]
21. Zhuk, N.A.; Sekushin, N.A.; Krzhizhanovskaya, M.G.; Kharton, V.V. Multiple relaxation, reversible electrical breakdown and bipolar conductivity of pyrochlore–type $Bi_2Cu_{0.5}Zn_{0.5}Ta_2O_9$ ceramics. *Solid State Ion.* **2022**, *377*, 115868. [CrossRef]
22. Zhuk, N.A.; Krzhizhanovskaya, M.G.; Koroleva, A.V.; Reveguk, A.A.; Sivkov, D.V.; Nekipelov, S.V. Thermal expansion, crystal structure, XPS and NEXAFS spectra of Fe-doped bismuth tantalate pyrochlore. *Ceram. Int.* **2022**, *48*, 14849–14855. [CrossRef]
23. Ismunandar; Kamiyama, T.; Oikawa, K.; Hoshikawa, A.; Kennedy, B.J.; Kubota, Y.; Kato, K. Static bismuth disorder in $Bi_{2-x}(CrTa)O_{7-y}$. *Mater. Res. Bull.* **2004**, *39*, 553–560. [CrossRef]
24. Jusoh, F.A.; Tan, K.B.; Zainal, Z.; Chen, S.K.; Khaw, C.C.; Lee, O.J. Investigation of structural and dielectric properties of subsolidus bismuth iron niobate pyrochlores. *J. Asian Ceram. Soc.* **2020**, *8*, 957–969. [CrossRef]
25. Tan, P.Y.; Tan, K.B.; Khaw, C.; Zainal, Z.; Chen, S.K.; Chon, M.P. Structural and electrical properties of bismuth magnesium tantalate pyrochlores. *Ceram. Int.* **2012**, *38*, 5401–5409. [CrossRef]
26. Youn, H.-J.; Sogabe, T.; Randall, C.A.; Shrout, T.R.; Lanagan, M.T. Phase Relations and Dielectric Properties in the Bi_2O_3-ZnO-Ta_2O_5 System. *J. Am. Ceram. Soc.* **2001**, *84*, 2557–2562. [CrossRef]
27. Khaw, C.C.; Tan, K.B.; Lee, C.K. High temperature dielectric properties of cubic bismuth zinc tantalate. *Ceram. Int.* **2009**, *35*, 1473–1480. [CrossRef]
28. Zhuk, N.A.; Krzhizhanovskaya, M.G.; Sekushin, N.A.; Kharton, V.V.; Koroleva, A.V.; Nekipelov, S.V.; Sivkov, D.V.; Sivkov, V.N.; Makeev, B.A.; Lebedev, A.M.; et al. Novel Ni-Doped Bismuth–Magnesium Tantalate Pyrochlores: Structural and Electrical Properties, Thermal Expansion, X-ray Photoelectron Spectroscopy, and Near-Edge X-ray Absorption Fine Structure Spectra. *ACS Omega* **2021**, *6*, 23262–23273. [CrossRef] [PubMed]
29. Rylchenko, E.P.; Makeev, B.A.; Sivkov, D.V.; Korolev, R.I.; Zhuk, N.A. Features of phase formation of pyrochlore-type $Bi_2Cr_{1/6}Mn_{1/6}Fe_{1/6}Co_{1/6}Ni_{1/6}Cu_{1/6}Ta_2O_{9+\Delta}$. *Lett. Mater.* **2022**, *12*, 486–492. [CrossRef]
30. Zhuk, N.; Makeev, B.; Krzhizhanovskaya, M.; Korolev, R. Effect of magnesium and zinc on phase formation of pyrochlore-type $Bi_2Mg(Zn)_{1-x}M_xTa_2O_{9.5-\Delta}$ (M-Cr, Fe) ceramics. *Ceram. Int.* **2023**, *49*, 5496–5509. [CrossRef]
31. Zhuk, N.A.; Kovalenko, S.Y.; Korolev, R.I.; Makeev, B.A.; Krzhizhanovskaya, M.G.; Sivkov, D.V.; Nekipelov, S.V.; Sivkov, V.N.; Yermolina, M.V. Features of Phase Formation of Pyrochlore-type Ceramics $Bi_2Mg(Zn)_{1-x}Ni_xTa_2O_9$. *ACS Omega* **2023**, *8*, 11351–11363. [CrossRef] [PubMed]
32. Akselrud, L.G.; Grin, Y.N.; Zavalij, P.Y. CSD-universal program package for single crystal or powder structure data treatment. *Thes. Rep. XII Eur. Crystallogr. Meet.* **1989**, *3*, 155.
33. Parshukova, K.N.; Rylchenko, E.P.; Muravyov, V.A.; Badanina, K.A.; Korolev, R.I.; Zhuk, N.A. Synthesis of Multicomponent Compounds with Pyrochloric Structure. *Glass Ceram.* **2023**, *79*, 418–421. [CrossRef]
34. Shannon, R.D. Revised effective ionic radii and systematic studies of interatomic distances in halides and chalcogenides. *Acta Crystallogr. A* **1976**, *32*, 751–767. [CrossRef]
35. Kato, K. Structure refinement of h-Nb_2O_5. *Acta Crystallogr. Sec. B Struct. Crystallogr. Cryst. Chem.* **1976**, *32*, 764–767. [CrossRef]
36. Zahid, A.H.; Han, Q. A review on the preparation, microstructure, and photocatalytic performance of Bi_2O_3 in polymorphs. *Nanoscale* **2021**, *13*, 17687–17724. [CrossRef]
37. Ling, C.D. Solving δ-Bi_2O_3-related superstructures by combining neutron powder diffraction and ab initio calculations. *Physica B* **2006**, *385–386*, 193–195. [CrossRef]
38. Gopalakrishnan, J.; Ramanan, A.; Rao, C.N.R.; Jefferson, D.A.; Smith, D.J. A homologous series of recurrent intergrowth structures of the type $Bi_4A_{m+n-2}B_{m+n}O_{3(m+n)+6}$ formed by oxides of the aurivillius family. *Solid State Chem.* **1984**, *55*, 101–105. [CrossRef]
39. Warda, S.A.; Pietzuch, W.; Massa, W.; Kesper, U.; Reinen, D. Color and Constitution of CrVI-Doped Bi_2O_3 Phases: The Structure of $Bi_{14}CrO_{24}$. *J. Solid State Chem.* **2000**, *149*, 209–217. [CrossRef]
40. Craid, D.C. Stephenson Structure Studies of Some Body-Centered Cubic Phase of Mixed Oxides Involving Bi_2O_3: The Structures of $Bi_{25}FeO_{40}$ and $Bi_{38}ZnO_{60}$. *J. Solid State Chem.* **1975**, *5*, 1–8.
41. Struzik, M.; Liu, X.; Abrahams, I.; Krok, F.; Malys, M.; Dygas, J.R. Defect structure and electrical conductivity in the pseudo-binary system Bi_3TaO_7–Bi_3NbO_7. *Solid State Ion.* **2012**, *218*, 25–30. [CrossRef]
42. Castro, A.; Aguado, E.; Rojo, J.M.; Herrero, P.; Enjalbert, R.; Galy, J. The New Oxygen-Deficient Fluorite Bi_3NbO_7: Synthesis, Electrical Behavior and Structural Approach. *Mater. Res. Bull.* **1998**, *33*, 31–41. [CrossRef]

43. Roth, R.S.; Waring, J.L. Synthesis and stability of bismutotantalite, stibiotantalite and chemically similar ABO_4 compounds. *Am. Mineral.* **1963**, *48*, 1348–1356.
44. Zhuk, N.A.; Krzhizhanovskaya, M.G.; Belyy, V.A.; Makeev, B.A. High-Temperature Crystal Chemistry of α-, β-, and γ-$BiNbO_4$ Polymorphs. *Inorg. Chem.* **2019**, *58*, 1518–1526. [CrossRef] [PubMed]
45. Guragain, D.; Zequine, C.; Gupta, R.K.; Mishra, S.R. Facile Synthesis of Bio-Template Tubular MCo_2O_4 (M = Cr, Mn, Ni) Microstructure and Its Electrochemical Performance in Aqueous Electrolyte. *Processes* **2020**, *8*, 343. [CrossRef]

Disclaimer/Publisher's Note: The statements, opinions and data contained in all publications are solely those of the individual author(s) and contributor(s) and not of MDPI and/or the editor(s). MDPI and/or the editor(s) disclaim responsibility for any injury to people or property resulting from any ideas, methods, instructions or products referred to in the content.